Eur. Phys. J. B **45**, 405–417 (2005)
DOI: 10.1140/epjb/e2005-00192-5

THE EUROPEAN PHYSICAL JOURNAL B

Spectroscopy of a driven solid-state qubit coupled to a structured environment

M.C. Goorden[1,a], M. Thorwart[2], and M. Grifoni[3]

[1] Instituut-Lorentz, Universiteit Leiden, P.O. Box 9506, 2300 RA Leiden, The Netherlands
[2] Institut für Theoretische Physik IV, Heinrich-Heine-Universität Düsseldorf, 40225 Düsseldorf, Germany
[3] Institut für Theoretische Physik, Universität Regensburg, 93035 Regensburg, Germany

Received 6 December 2004
Published online 6 July 2005 –

Abstract. We study the asymptotic dynamics of a driven spin-boson system where the environment is formed by a broadened localized mode. Upon exploiting an exact mapping, an equivalent formulation of the problem in terms of a quantum two-state system (qubit) coupled to a harmonic oscillator which is itself Ohmically damped, is found. We calculate the asymptotic population difference of the two states in two complementary parameter regimes. For weak damping and low temperature, a perturbative Floquet-Born-Markovian master equation for the qubit-oscillator system can be solved. We find multi-photon resonances corresponding to transitions in the coupled quantum system and calculate their line-shape analytically. In the complementary parameter regime of strong damping and/or high temperatures, non-perturbative real-time path integral techniques yield analytic results for the resonance line shape. In both regimes, we find very good agreement with exact results obtained from a numerical real-time path-integral approach. Finally, we show for the case of strong detuning between qubit and oscillator that the width of the n-photon resonance scales with the nth Bessel function of the driving strength in the weak-damping regime.

PACS. 03.65.Yz Decoherence; open systems; quantum statistical methods – 03.67.Lx Quantum computation – 74.50.+r Tunneling phenomena; point contacts, weak links, Josephson effects – 42.50.Hz Strong-field excitation of optical transitions in quantum systems; multiphoton processes; dynamic Stark shift

1 Introduction

Currently, we witness an impressive progress in realizing coherent quantum dynamics of macroscopic solid state devices [1–5]. Very recently, experimental results on the quantum dynamics of a superconducting flux qubit coupled to a read-out SQUID have been reported [6]. The flux qubit consists of a superconducting ring with three Josephson junctions and, in the proper parameter regime, it forms a quantum mechanical macroscopic two-state system (TSS). An external time-dependent driving force controls the state of the TSS. A SQUID couples inductively to the qubit and, together with an external shunt capacitance, it can be modeled as a harmonic oscillator (HO). Due to the coupling of the SQUID to the surrounding environment, the harmonic oscillator is (weakly) damped. The state of the qubit can be inferred from the state of the SQUID. The experiment provides spectroscopic data on the different transition frequencies of the coupled TSS-HO device. Moreover, Rabi oscillations involving different pairs of quantum states of the device have been revealed, including the so-termed red and blue sideband transitions between energy states of the coupled TSS-HO system.

Heading for a comprehensive detailed understanding, a quantitative modeling which includes the effects of time-dependent driving, decoherence and dissipation is required. Our description goes beyond the well-known Jaynes-Cummings model [7], by avoiding the strong rotating-wave approximation and by including a microscopic model for the environment. A generic theoretical model for studying the environmental effects on a driven TSS is the driven spin-boson model [8,9] where the TSS tunneling splitting is denoted by Δ. The environment is characterized by a spectral density $J(\omega)$. The widest used form is that of an Ohmic spectral density, where $J(\omega)$ is proportional to the frequency ω. It mimics the effects of an unstructured Ohmic electromagnetic environment. In the classical limit this leads to white noise and all transitions in the system are damped equally. However, if the environment for the qubit is formed by a quantum measuring device which itself is damped by Ohmic fluctuations, the simple description as an Ohmic environment might become inappropriate. In particular, the SQUID-detector being well described as a HO can equally well be considered

[a] e-mail: goorden@lorentz.leidenuniv.nl

as a (broadened) localized mode of the environment influencing the qubit as the central quantum system. In this picture, the plasma resonance at frequency Ω_p of the SQUID gives rise to a non-Ohmic effective spectral density $J_{\rm eff}(\omega)$ for the qubit with a Lorentzian peak at the plasma frequency of the detector [10].

The effects of such a structured spectral density on decoherence have been investigated in several theoretical works in various limits. The role of the external driving being in resonance with the symmetric TSS at zero temperature has been studied in reference [11] within a Bloch-Redfield formalism being equivalent to a perturbative approach in $J_{\rm eff}$. Smirnov's analysis [12] is based on the assumption of weak interaction between the TSS and the HO being equivalent to a perturbative approach in $J_{\rm eff}$ as well. Moreover, a rotating-wave approximation is used. The first assumption, however, might become problematic if the driven TSS is in resonance with the HO. The results presented in references [13,14] reveal in fact, for the undriven case, that a perturbative approach in $J_{\rm eff}$ breaks down for strong qubit-detector coupling, and when the qubit and detector frequencies are comparable. Dephasing times at zero temperature have been determined for the undriven spin-boson model with a structured environment in reference [15] within a numerical flow equation method.

The interplay between the external driving and the dynamics of the coupled TSS-HO system yields to additional multi-photon transitions, which can be explained only by considering the spectrum of the coupled system. These resonances have recently been observed experimentally [6]. If the time-scale of the HO does not play a role, the multi-photon resonances occur in the driven qubit solely, which happens when the driving frequency (or integer multiples of it) matches the characteristic energy scales of the qubit [9]. Such multiphoton resonances can be experimentally detected in an ac-driven flux qubit by measuring the asymptotic occupation probabilities of the qubit, as the dc-field is varied [16]. In these experiments the resonances were obtained by matching the frequency of the ac-field with the qubit energy levels only, where the detector energy levels did not play a role. These qubit resonances, which have also been theoretically investigated within a Bloch equation formalism in reference [17], could be explained in terms of intrinsic transitions in a driven spin-boson system with an unstructured environment.

In this paper, we provide a comprehensive theoretical description of the driven spin-boson system in the presence of a structured environment with one localized mode. Upon making use of the equivalence of this generic model with the model of a driven TSS coupled to an Ohmically damped HO, we first consider the experimentally most interesting case of low temperature and weak damping of the HO while the coupling between the TSS and the HO is kept arbitrary. In this regime, a Floquet-Born-Markov master equation can be established for the driven TSS-HO system. A restriction to the most relevant energy states allows the analytic calculation of the asymptotic TSS time-averaged population P_∞, including the explicit shape of the resonance peaks and dips. We furthermore consider the case of strong damping and/or high temperature which is the complementary parameter regime. An analytic real-time path-integral approach within the non-interacting blip approximation for the driven TSS with the Lorentzian-shaped spectral density allows to analytically determine P_∞ as well. We compare the results obtained from closed analytic expressions with those of numerically exact real-time QUAPI calculations in both parameter regimes and find a very good agreement validating our analytical approaches. Finally, we consider the weakly damped TSS with the localized mode in the limit of large HO frequencies. Then, the localized mode acts as a high-frequency cutoff and the usual Ohmically damped driven TSS is recovered. For this case, we employ an approximation valid for large driving frequencies and obtain a simple expression for the resonance line shapes for multi-photon transitions. Most importantly, we find that the width of the n-photon resonance scales with the nth ordinary Bessel function. Parts of our results have been published in a short work in reference [18].

The paper is organized as follows: In Section 2, we present the theoretical model. Then, we treat the regime of weak damping and low temperatures in Section 3. The complementary regime of strong damping is investigated in Section 4. The subsequent Section 5 contains the limit when the localized mode provides a high-frequency cut-off for the bath, and Section 6 the discussion of the results and the conclusions. Details of the specific evaluation of rate coefficients are presented in Appendix A. In Appendix B an expansion used in the strong coupling regime is elaborated in detail.

2 The driven qubit coupled to a macroscopic detector

The driven TSS is described by the Hamiltonian

$$H_Q(t) = -\frac{\hbar\Delta}{2}\sigma_x - \frac{\hbar\varepsilon(t)}{2}\sigma_z, \tag{1}$$

where σ_i are Pauli matrices, $\hbar\Delta$ is the tunnel splitting, and $\varepsilon(t) = \varepsilon_0 + s\cos(\Omega t)$ describes the combined effects of a time-dependent driving and the static bias ε_0. In the absence of ac-driving ($s = 0$), the level splitting of the isolated TSS is given by

$$\hbar\nu = \hbar\sqrt{\varepsilon_0^2 + \Delta^2}. \tag{2}$$

The detector can be associated as part of the TSS environment as a localized mode. This gives the spin-boson Hamiltonian H_{SB} reading [8,9,11–15]

$$H_{SB}(t) = H_Q(t) + \frac{1}{2}\sigma_z\hbar\sum_k \tilde{\lambda}_k(\tilde{b}_k^\dagger + \tilde{b}_k) + \sum_k \hbar\tilde{\omega}_k\tilde{b}_k^\dagger\tilde{b}_k. \tag{3}$$

Here $\tilde{b}_k$ and $\tilde{b}_k^\dagger$ are annihilation and creation operators of the kth bath mode with frequency $\tilde{\omega}_k$. The presence of the detector determines the shape of the spectral density. Following reference [10], the dc-SQUID can be modeled as an effective inductance which is shunted with an on-chip capacitance. This gives rise to the effective spectral density

$$J_{\rm eff}(\omega) = \sum_k \tilde{\lambda}_k^2 \delta(\omega - \tilde{\omega}_k) = \frac{2\alpha\omega\Omega_p^4}{(\Omega_p^2 - \omega^2)^2 + (2\pi\kappa\omega\Omega_p)^2} \quad (4)$$

of the bath having a Lorentzian peak of width $\gamma = 2\pi\kappa\Omega_p$ at the characteristic detector frequency Ω_p. It behaves Ohmically at low frequencies with the dimensionless coupling strength $\alpha = \lim_{\omega\to 0} J_{\rm eff}(\omega)/2\omega$. The qubit dynamics is described by the reduced density operator $\rho(t)$ obtained by tracing out the bath degrees of freedom. The relevant observable which corresponds to the experimentally measured switching probability of the SQUID bias current is the population difference $P(t) := \langle\sigma_z\rangle(t) = {\rm tr}[\rho(t)\sigma_z]$ between the two localized states of the qubit. We focus on the asymptotic value averaged over one period of the external driving field, i.e., $P_\infty = \lim_{t\to\infty}\langle P(t)\rangle_\Omega$.

In the following, it will become clear that it is convenient to exploit the exact one-to-one mapping [19] of the Hamiltonian (3) onto that of a driven TSS coupled to a single harmonic oscillator mode with frequency Ω_p with interaction strength g. The HO itself interacts with a set of mutually non-interacting harmonic oscillators. The corresponding total Hamiltonian is then

$$H_{QOB}(t) = H_{QO}(t) + H_{OB} \quad (5)$$

with

$$H_{QO}(t) = H_Q(t) + \hbar g\sigma_z(B^\dagger + B) + \hbar\Omega_p B^\dagger B,$$
$$H_{OB} = (B^\dagger + B)\sum_k \hbar\nu_k(b_k^\dagger + b_k) + \sum_k \hbar\omega_k b_k^\dagger b_k + (B^\dagger + B)^2 \sum_k \hbar\frac{\nu_k^2}{\omega_k}, \quad (6)$$

where we have omitted the zero-point constant energy terms. Here, B and $B^\dagger$ are the annihilation and creation operators of the localized HO mode, while b_k and $b_k^\dagger$ are the corresponding bath mode operators. The spectral density of the continuous bath modes is now Ohmic with dimensionless damping strength κ, i.e.,

$$J_{\rm Ohm}(\omega) = \sum_k \nu_k^2\delta(\omega - \omega_k) = \kappa\omega\frac{\omega_D^2}{\omega^2 + \omega_D^2}, \quad (7)$$

where we have introduced a high-frequency Drude cut-off at frequency ω_D. If ω_D is larger than all other energy scales the particular choice of cut-off does not influence the results at long times. The relation between g and α follows as $g = \Omega_p\sqrt{\alpha/(8\kappa)}$. Figure 1 illustrates a sketch of the two

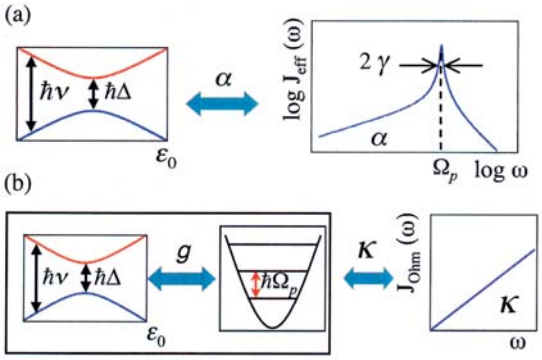

Fig. 1. Schematic picture of the models we use. In (a) the TSS is coupled to an environment which has a peaked spectral density $J_{\rm eff}(\omega)$. In (b) the system is shown as a two-level system coupled to a harmonic oscillator which is itself coupled to an Ohmic environment with spectral density $J_{\rm Ohm}(\omega)$.

equivalent descriptions of the system. Figure 1a shows the viewpoint where the localized mode is part of the environmental modes, while Figure 1b depicts the perspective of the localized mode being part of the "central" quantum system which itself is coupled to an Ohmic environment. The equivalence of both standpoints has first been pointed out by Garg et al. [19] in the context of electron transfer in chemical physics. As shown below, the first way is more convenient for the description in terms of analytic real-time path-integrals (Sect. 4), while the second viewpoint is more appropriate for the regime of weak-coupling and for the numeric treatment with QUAPI (see below). Note that the TSS reduced density operator $\rho(t)$ is obtained after tracing out the degrees of freedom of the bath and of the HO. Further progress relies on approximations which depend on the choice of the various parameters.

3 Weak coupling: Floquet-Born-Markov master equation

If the coupling between the HO and the bath is weak, i.e., $\kappa \ll 1$, we can choose an approach in terms of a Born-Markov master equation in an extended Floquet description [9,20,21]. For a self-contained discussion, we shortly introduce below the required formalism of the Floquet theory. The interested reader can find more details in the review in reference [9].

3.1 Floquet formalism and Floquet-Born-Markovian master equation

For systems with periodic driving it is convenient to use the Floquet formalism that allows to treat periodic forces of arbitrary strength and frequency [20]. It is based on the fact that the eigenstates of a periodic Hamiltonian $H_{QO}(t) = H_{QO}(t + 2\pi/\Omega)$ are of the form

$$|\psi(t)\rangle = e^{-i\varepsilon_\alpha t/\hbar}|\phi_\alpha(t)\rangle,$$
$$|\phi_\alpha(t)\rangle = |\phi_\alpha(t + 2\pi/\Omega)\rangle, \quad (8)$$

with the Floquet states $|\phi_\alpha(t)\rangle$ being periodic in time (as is the Hamiltonian) and ε_α are called the Floquet or quasi-energies. They can be obtained from the eigenvalue equation

$$\left(H_{QO}(t) - i\hbar\frac{\partial}{\partial t}\right)|\phi_\alpha(t)\rangle = \varepsilon_\alpha|\phi_\alpha(t)\rangle. \tag{9}$$

If the quasi-energy ε_α is an eigenvalue with Floquet state $|\phi_\alpha(t)\rangle$, so is $\varepsilon_\alpha + n\hbar\Omega$ with Floquet state $\exp(in\Omega t)|\phi_\alpha(t)\rangle$. Both Floquet states correspond to the same physical state. Because of their periodicity both the Floquet states and the Hamiltonian can be written as a Fourier series, i.e.,

$$\begin{aligned}|\phi_\alpha(t)\rangle &= \sum_n |\phi_\alpha^{(n)}\rangle \exp(in\Omega t),\\ H_{QO}(t) &= \sum_n H_{QO}^{(n)} \exp(in\Omega t).\end{aligned} \tag{10}$$

Substituting these Fourier decompositions in the eigenvalue equation (9) gives [22]

$$\sum_k (H_{QO}^{(n-k)} + n\hbar\Omega\delta_{kn})\phi_\alpha^{(k)} = \varepsilon_\alpha\phi_\alpha^{(n)}. \tag{11}$$

This allows us to define the Floquet Hamiltonian $\mathcal{H}_{QO} \equiv H_{QO}(t) - i\hbar\frac{\partial}{\partial t}$ in matrix form with the matrix elements

$$\langle an|\mathcal{H}_{QO}|bm\rangle = (H_{QO}^{(n-m)})_{ab} + n\hbar\Omega\delta_{ab}\delta_{nm}. \tag{12}$$

In the notation $|an\rangle$, a refers to a basis in which to express the Hamiltonian $H_{QO}(t)$, while n refers to the Fourier coefficient. The eigenvectors of $\mathcal{H}_{QO}$ are the coefficients $\phi_\alpha^{(n)}$.

The dynamics of the system coupled to a harmonic bath is conveniently described by an equation of motion for the density matrix ρ. Driving effects can be captured in an elegant way by formulating the equation of motion in the basis of Floquet states defined in equation (8). For weak coupling to the environment, it is sufficient to include dissipative effects to lowest order in κ. Within this approximation, a Floquet-Born-Markov master equation has been established [9,20,21]. We average the $2\pi/\Omega$-periodic coefficients of the master equation over one period of the driving, assuming that dissipative effects are relevant only on timescales much larger than $2\pi/\Omega$. This yields equations of motion for the reduced density matrix $\rho_{\alpha\beta}(t) = \langle\phi_\alpha(t)|\rho(t)|\phi_\beta(t)\rangle$ of the form

$$\dot\rho_{\alpha\beta}(t) = -\frac{i}{\hbar}(\varepsilon_\alpha - \varepsilon_\beta)\rho_{\alpha\beta}(t) + \sum_{\alpha'\beta'} L_{\alpha\beta,\alpha'\beta'}\rho_{\alpha'\beta'}(t), \tag{13}$$

with the dissipative transition rates

$$\begin{aligned}L_{\alpha\beta,\alpha'\beta'} = &\sum_n (N_{\alpha\alpha',n} + N_{\beta\beta',n})X_{\alpha\alpha',n}X_{\beta'\beta,-n}\\ &- \delta_{\beta\beta'}\sum_{\beta'',n} N_{\beta''\alpha',n}X_{\alpha\beta'',-n}X_{\beta''\alpha',n}\\ &- \delta_{\alpha\alpha'}\sum_{\alpha'',n} N_{\alpha''\beta',n}X_{\beta'\alpha'',-n}X_{\alpha''\beta,n}.\end{aligned} \tag{14}$$

Here, we have defined

$$\begin{aligned}X_{\alpha\beta,n} &= \sum_k \langle\phi_\alpha^{(k)}|B + B^\dagger|\phi_\beta^{(k+n)}\rangle,\\ N_{\alpha\beta,n} &= N(\varepsilon_\alpha - \varepsilon_\beta + n\hbar\Omega),\\ N(\varepsilon) &= \frac{\kappa\varepsilon}{2\hbar}\left(\coth\left(\frac{\varepsilon}{2k_BT}\right) - 1\right).\end{aligned} \tag{15}$$

We have neglected the weak quasi-energy shifts, which are of first order in the coupling to the environment. In the sequel, we will see from a comparison with exact numerical results that this approximation is well justified. In order to be able to solve equation (13), it is necessary to determine the Floquet quasi-energies ε_α and Floquet states $|\phi_\alpha^{(n)}\rangle$. How they can be determined perturbatively, is shown in the following subsection.

3.2 Van Vleck perturbation theory

First, we have to specify the basis for the Floquet Hamiltonian according to equation (12). For the TSS+HO Hamiltonian H_{QO}, we use the basis $|an\rangle$ defined via the single particle product state $|a\rangle = |g/e\, m\rangle$ with $|g/e\rangle$ being the ground/excited state of the qubit, $|m\rangle$ the HO eigenstate, and n the corresponding Fourier index. In detail, this implies that we can divide the Hamiltonian into a diagonal part

$$\begin{aligned}(\mathcal{H}_{QO})_{gmn,gmn} &= \hbar[-\nu/2 + m\Omega_p + n\Omega],\\ (\mathcal{H}_{QO})_{emn,emn} &= \hbar[\nu/2 + m\Omega_p + n\Omega],\end{aligned} \tag{16}$$

and an off-diagonal part

$$(\mathcal{H}_{QO})_{an,bk} = V_{an,bk}, \quad \text{for } a \neq b, n \neq k, \tag{17}$$

which has non-zero elements. They read

$$\begin{aligned}V_{g(e)ln,g(e)mn} &= +(-)\frac{(\sqrt{m+1}\delta_{l,m+1} + \sqrt{l+1}\delta_{l+1,m})\hbar g\varepsilon_0}{\nu},\\ V_{g(e)ln,e(g)mn} &= -\frac{(\sqrt{m+1}\delta_{l,m+1} + \sqrt{l+1}\delta_{l+1,m})\hbar g\Delta}{\nu},\\ V_{g(e)mn,g(e)mk} &= -(+)\frac{(\delta_{k,n+1} + \delta_{k+1,n})\hbar s\varepsilon_0}{4\nu},\\ V_{g(e)mn,e(g)mk} &= \frac{(\delta_{k,n+1} + \delta_{k+1,n})\hbar s\Delta}{4\nu}.\end{aligned} \tag{18}$$

In the remainder of this section we will assume that the elements of V are small compared to the diagonal elements of $\mathcal{H}_{QO}$, which is justified if the coupling g between TSS and HO and the driving amplitude s are small compared to the other energy scales, i.e., $s, g \ll \Omega, \nu, \Omega_p$. This is the case in realistic experimental devices [6,13]. The Fourier index n ranges from $-\infty$ to ∞ and m from 0 to ∞. The eigenvalues of the Floquet Hamiltonian following from equations (17) and (18) have to be calculated numerically for a particular cut-off n_{max} and m_{max}. In Figure 2, the numerically obtained quasi-energy spectrum is shown

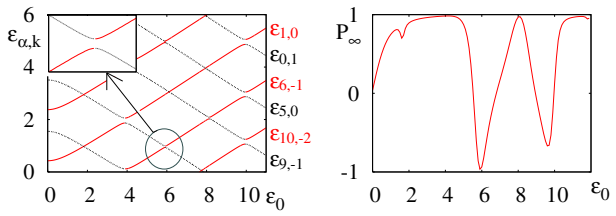

Fig. 2. Left: Quasi-energy spectrum $\varepsilon_{\alpha,k}$ of the driven TSS+HO system vs. dc-bias ε_0 (in units of Δ). The quasi-energies are defined up to an integer multiple of $\hbar\Omega$, i.e., $\varepsilon_{\alpha,k} = \varepsilon_\alpha + k\hbar\Omega$. Inset: Zoom of an anti-crossing. Right: P_∞ exhibits resonance dips corresponding to quasi-energy level anti-crossings. Parameters are $\Omega = 10\Delta, s = 4\Delta, g = 0.4\Delta, \Omega_p = 4\Delta, \kappa = 0.014$ and $k_BT = 0.1\hbar\Delta$.

as a function of the static bias ε_0 for the case $m_{\max} = 4$ and $|n_{\max}| = 8$. We find that for some values of the bias ε_0 avoided crossings of the quasienergy levels occur when two diagonal elements of $\mathcal{H}_{QO}$ have approximately the same values, i.e., when the condition

$$E_{an,bm} := (\mathcal{H}_{QO})_{an,an} - (\mathcal{H}_{QO})_{bm,bm} = 0 + O(V^2) \quad (19)$$

is fulfilled. It follows from equation (17) that this happens when at least one of the two conditions

$$\begin{aligned} \nu &= n\Omega \pm m\Omega_p + O(V^2), \\ n\Omega &= m\Omega_p + O(V^2), \end{aligned} \quad (20)$$

is fulfilled. At these avoided crossings the Floquet spectrum has quasi-degeneracies and as a consequence there are transitions between the different Floquet states. As it turns out below, this results in resonant peaks/dips in the stationary averaged population difference P_∞, cf. Figure 2.

Since we are interested in describing the resonance line shape for P_∞, we have to determine the quasi-energies and Floquet states around a resonance, i.e., around an avoided crossing. For this, we use an approach which is perturbative in V. The unperturbed Hamiltonian is diagonal and, close to an avoided crossing, (nearly) degenerate. An appropriate perturbative method is the Van Vleck perturbation theory [7,23] suitable for Hamiltonians for which the unperturbed spectrum has groups of (nearly) degenerate eigenvalues, well separated in energy space. An example of such a spectrum is shown in Figure 3. This method defines a unitary transformation which transforms the Hamiltonian into an effective block-diagonal one. The effective Hamiltonian then has the same eigenvalues as the original Hamiltonian, with the quasi-degenerate eigenvalues in one common block.

The effective Hamiltonian can be written as

$$\mathcal{H}_{\text{eff}} = e^{iS}\mathcal{H}_{QO}e^{-iS}. \quad (21)$$

In reference [7] it is shown how to obtain S systematically for every order in the perturbation. The small parameter is $V/\Delta E_2$ (see Fig. 3). Eigenvalues within one block can be arbitrarily close. This means that we can also use the expansion at resonance. We derive the expressions up to the

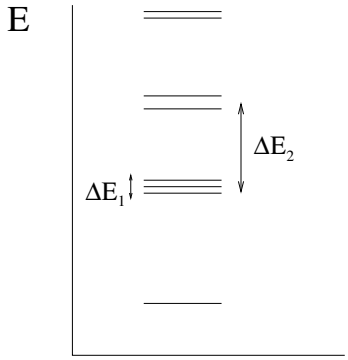

Fig. 3. Typical energy spectrum suited for the Van Vleck perturbation theory: Different groups of (nearly) degenerate levels of eigenenergies are well separated in energy (i.e., $\Delta E_1 \ll \Delta E_2$).

second order in the perturbation. Two different cases are relevant: For the case when $(\mathcal{H}_{QO})_{an,an}$ and $(\mathcal{H}_{QO})_{bm,bm}$ are not nearly degenerate we find

$$\begin{aligned} iS^{(1)}_{an,bm} &= \frac{V_{an,bm}}{E_{an,bm}}, \\ iS^{(2)}_{an,bm} &= \sum_{c,k} \frac{V_{an,ck}V_{ck,bm}}{2E_{bm,an}} \left(\frac{1}{E_{ck,an}} + \frac{1}{E_{ck,bm}} \right), \end{aligned} \quad (22)$$

where the superscript indicates the order of perturbation theory. For the second case when $(\mathcal{H}_{QO})_{an,an}$ and $(\mathcal{H}_{QO})_{bm,bm}$ are nearly degenerate, we find $iS^{(1)}_{an,bm} = iS^{(2)}_{an,bm} = 0$.

In turn, the matrix elements of the nth order term $\mathcal{H}^{(n)}_{\text{eff}}$ of the effective Hamiltonian can be calculated, again for both cases. When $(\mathcal{H}_{QO})_{an,an}$ and $(\mathcal{H}_{QO})_{bm,bm}$ are not nearly degenerate, we find $(\mathcal{H}_{\text{eff}})^{(1)}_{an,bm} = (\mathcal{H}_{\text{eff}})^{(2)}_{an,bm} = 0$. For the second case, when $(\mathcal{H}_{QO})_{an,an}$ and $(\mathcal{H}_{QO})_{bm,bm}$ are nearly degenerate, one finds

$$\begin{aligned} (\mathcal{H}_{\text{eff}})^{(1)}_{an,bm} &= V_{an,bm}, \\ (\mathcal{H}_{\text{eff}})^{(2)}_{an,bm} &= \frac{1}{2}\sum_{c,k} V_{an,ck}V_{ck,bm} \left(\frac{1}{E_{an,ck}} + \frac{1}{E_{bm,ck}} \right). \end{aligned} \quad (23)$$

Since the effective block-diagonal Hamiltonian consequently only has 2×2 blocks, it is easy to diagonalize it. To obtain the eigenvectors of the original Floquet Hamiltonian (see Eqs. (17, 18)), the inverse of the transformation defined in equation (21) has to be performed on the eigenvectors. There is an infinite number of quasienergy levels and Floquet states. However, because the eigenvalues ε_α and $\varepsilon_\alpha + n\hbar\Omega$ represent the same physical state, only one of them has to be considered. Still there is an infinite number of levels because the Hilbert space of the HO Hamiltonian is infinite dimensional. Nevertheless, for practical calculations, only the relevant HO levels have to

$$H_{\rm eff} = \hbar \begin{pmatrix} \frac{\nu}{2} + \Omega_p - \Omega + W_1 & -\Delta_1 & 0 & 0 \\ -\Delta_1 & -\frac{\nu}{2} + W_2 & 0 & 0 \\ 0 & 0 & -\frac{\nu}{2} + \Omega_p + W_3 & 0 \\ 0 & 0 & 0 & \frac{\nu}{2} + W_4 \end{pmatrix}. \tag{25}$$

be taken into account. When there is a resonance between the states $|e/g, 0, n\rangle$ and $|e/g, l, n+k\rangle$, then at least the first l levels of the HO play a role. Higher levels can be omitted if one is interested in low temperatures, which is commonly the case, since for low temperatures their occupation number will be very small.

3.3 Line shape of the resonant peak/dip

To obtain the line shape of the resonant peak/dip in P_∞, we have to determine the stationary solution of equation (13). Depending on the number n_{max} of Floquet states taken into consideration, this might be considerably difficult. One facilitation might arise due to symmetries, i.e., elements of $L_{\alpha\beta,\alpha'\beta'}$ being of the same size. Another possibility appropriate at low temperatures might be to neglect some of the dissipative transition rates. Moreover, a further possible approximation can be applied for $\rho_{\alpha\beta}(\infty)$, if ε_α and ε_β are not nearly-degenerate eigenvalues. In that case $\varepsilon_\alpha - \varepsilon_\beta$ in equation (13) is much larger than the coefficients $L_{\alpha\beta\alpha'\beta'}$, since the coupling to the Ohmic environment is assumed to be weak. This, in turn, allows to make the partial secular approximation by setting $\rho_{\alpha\beta}(\infty) = 0$. After the reduced density matrix in the Floquet basis is known, it is straightforward to calculate P_∞.

3.4 Example: The first blue sideband

As an example we will derive an analytical expression for the resonant dip at $\nu \approx \Omega - \Omega_p$ which is called the first blue sideband. For this case, the matrix elements $(\mathcal{H}_{QO})_{g0\,n+1,g0\,n+1}$ and $(\mathcal{H}_{QO})_{e1n,e1n}$ are nearly degenerate, i.e.,

$$-\nu/2 + (n+1)\Omega \approx \nu/2 + \Omega_p + n\Omega. \tag{24}$$

As the resonance occurs between two states which differ only by one oscillator quantum, we only take into account one excited level of the oscillator. We expect that this is a reasonable approximation for not too strong driving and low temperatures. The validity of this approximation will be checked against numerically exact results in the end. The elements of the transformation matrix S follow as $S_{g0\,n+1,e1n} = S_{e1n,g0\,n+1} = 0$, while the remaining elements can be calculated straightforwardly using equation (22) and they will not be given here explicitly.

Since we include one HO excited energy level, we have four physically different eigenstates. Hence, we can express $\mathcal{H}_{QO}$ in the basis $\{|e,1,-1\rangle, |g,0,0\rangle, |g,1,0\rangle, |e,0,0\rangle\}$. Performing the transformation defined in equation (21), we obtain the effective Hamiltonian in this basis as

See equation (25) above.

The matrix elements are calculated using equation (23). They read

$$\begin{aligned} \Delta_1 &= \frac{\Delta\varepsilon_0 gs\left[\Omega^2 + \Omega_p^2 + \nu(-\Omega + \Omega_p)\right]}{4\nu(\Omega - \nu)\Omega\,\Omega_p(\nu + \Omega_p)}, \\ W_1 = -W_2 &= \frac{\varepsilon_0^2 g^2}{\nu^2\Omega_p} + \frac{\Delta^2 g^2}{\nu^2(\nu + \Omega_p)} + \frac{\Delta^2 s^2}{8\nu(\nu^2 - \Omega^2)}, \\ W_3 = -W_4 &= \frac{\varepsilon_0^2 g^2}{\nu^2\Omega_p} - \frac{\Delta^2 g^2}{\nu^2(\nu - \Omega_p)} - \frac{\Delta^2 s^2}{8\nu(\nu^2 - \Omega^2)}. \end{aligned} \tag{26}$$

The eigenvalues of the Hamiltonian (25) are the relevant quasi-energies, and they are readily obtained by diagonalization as

$$\begin{aligned} \frac{\varepsilon_{1/2}}{\hbar} &= -\frac{\nu}{2} + \frac{\delta}{2}\left(1 \mp \sqrt{1 + \frac{\Delta_1^2}{\delta^2}}\right) - W_1, \\ \frac{\varepsilon_3}{\hbar} &= -\frac{\nu}{2} + \Omega_p + W_3, \\ \frac{\varepsilon_4}{\hbar} &= \frac{\nu}{2} + W_4. \end{aligned} \tag{27}$$

From these formulas it follows that $\delta = \nu - \Omega + \Omega_p + 2W_1$ is a measure of how far the system is off resonance. For $\delta = 0$, the quasi-energies ε_1 and ε_2 show an avoided crossing of size $\hbar\Delta_1$. Note that equation (13) implies that Δ_1 is the Rabi frequency at the blue sideband.

The eigenvectors, which are the Floquet states, of the 4×4 effective block-diagonal matrix in equation (25) are easily obtained by performing the corresponding inverse transformation. We find, with $\tan\theta = 2|\Delta_1|/\delta$, the eigenstates

$$\begin{aligned} |\phi_1\rangle &= e^{-iS}[\sin(\theta/2)e^{-i\Omega t}|e,1\rangle + \cos(\theta/2)|g,0\rangle], \\ |\phi_2\rangle &= e^{-iS}[\cos(\theta/2)e^{-i\Omega t}|e,1\rangle - \sin(\theta/2)|g,0\rangle], \\ |\phi_{3/4}\rangle &= e^{-iS}|g/e,1/0\rangle. \end{aligned} \tag{28}$$

We have used the inverse transformation of equation (10) to illustrate the time-dependence explicitly. Next, we calculate the rates given in equation (14) up to second order in V.

The quasi-energies ε_1 and ε_2 are quasi-degenerate. To be definite, we assume a *partial secular approximation*: We set almost all off-diagonal elements of ρ to zero but keep $\rho_{12}(\infty)$ and $\rho_{21}(\infty) = \rho_{12}^*(\infty)$ different from zero. This allows to simplify the master equation (13). The stationary

solutions are determined by the conditions

$$0 = \sum_\beta L_{\alpha\alpha,\beta\beta}\rho_{\beta\beta}(\infty) + (L_{\alpha\alpha,12} + L_{\alpha\alpha,21})\mathrm{Re}[\rho_{12}(\infty)],$$
$$0 = -\frac{i}{\hbar}(\varepsilon_1 - \varepsilon_2)\rho_{12}(\infty) + \sum_\alpha L_{12,\alpha\alpha}\rho_{\alpha\alpha}(\infty) + L_{12,12}\rho_{12}(\infty) + L_{12,21}\rho^*_{12}(\infty). \quad (29)$$

It is most convenient to use the symmetry properties of the corresponding rates which are specified for this particular example in the equations (A.1) in Appendix A. In turn, there are eight independent rates associated to all possible transitions. They are explicitly given in the equations (A.2).

First we consider the rates exactly at resonance $\delta = 0$. Since then $\sin^2(\theta/2) = \cos^2(\theta/2) = 1/2$, all rates contain a term which is of zeroth order in V. If we neglect the small second order terms, we find

$$\begin{aligned}
L_{22,44} &= L_{11,44} = L_{33,22} = L_{33,11} = -L_{33,21} \\
&= L_{21,44} = N(\hbar\Omega_p), \\
L_{22,33} &= L_{11,33} = L_{44,22} = L_{44,11} = L_{44,21} \\
&= -L_{21,33} = N(-\hbar\Omega_p), \\
L_{11,21} &= L_{22,21} = L_{21,22} = L_{21,11} \\
&= \frac{1}{2}[N(\hbar\Omega_p) - N(-\hbar\Omega_p)], \\
L_{12,12} &= -N(-\hbar\Omega_p) - N(\hbar\Omega_p). \quad (30)
\end{aligned}$$

Solving equation (29) together with (30) finally yields

$$\begin{aligned}
\rho_{11}(\infty) &= \rho_{22}(\infty) = \frac{N(-\hbar\Omega_p)N(\hbar\Omega_p)}{[N(-\hbar\Omega_p) + N(\hbar\Omega_p)]^2}, \\
\rho_{33}(\infty) &= \frac{N(\hbar\Omega_p)^2}{[N(-\hbar\Omega_p) + N(\hbar\Omega_p)]^2}, \\
\rho_{44}(\infty) &= \frac{N(-\hbar\Omega_p)^2}{[N(-\hbar\Omega_p) + N(\hbar\Omega_p)]^2}, \\
\rho_{12}(\infty) &= 0. \quad (31)
\end{aligned}$$

Eventually, this gives the simple result at resonance, $\delta = 0$,

$$P_\infty = -\frac{\varepsilon_0}{\nu}\tanh\left(\frac{\hbar\Omega_p}{2k_BT}\right) + O\left(V^2\right), \quad (32)$$

which implies a complete inversion of population at low temperatures! We will discuss the physics of this in Section 3.5. Note that no further assumption on the temperature was made while deriving this formula.

Next we will derive an expression for the peak shape around the resonance. For this, we assume low temperatures, i.e., $k_BT/\hbar \ll \Omega_p, \Omega, \nu$. This allows us to set $N(\hbar\Omega_p) = N(\hbar\Omega) = N(\hbar\nu) = 0$. Far enough away from resonance, it is appropriate to assume that $\rho_{12}(\infty) \approx \rho_{21}(\infty) \approx 0$, and $\sin(\theta/2) \approx \theta/2$. Thus, it follows from equation (A.1) that there are only four independent rates in this case, namely $L_{44,22}, L_{22,44}, L_{44,11}$ and $L_{11,44}$.

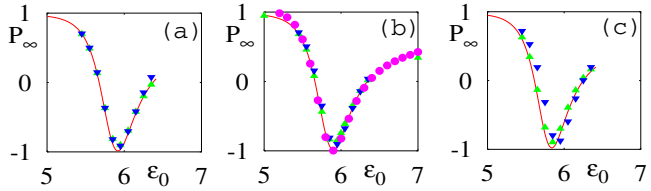

Fig. 4. P_∞ vs. ε_0 (in units of Δ) around the peak at $\nu = \Omega - \Omega_p$. The solid lines are the analytical prediction (35) for (a) $g = 0.05\Delta$, (b) $g = 0.2\Delta$, (c) $g = 0.4\Delta$. The triangles are the results of a Floquet-Bloch-Redfield simulation, cf. equation (13), with one (upward triangles) and two (downward triangles) HO levels taken into account. The circles in (b) are the results from a QUAPI simulation with six HO levels (see text). We choose $s = 2\Delta$, $\Omega = 10\Delta$, $\kappa = 0.014$, $k_BT = 0.1\hbar\Delta$.

Within our approximations, we find that $L_{22,44} = O(V^3)$. So only three rates are relevant which read

$$\begin{aligned}
L_{44,22} &= 2\cos^2(\theta/2) \approx 2, \\
L_{11,44} &= 2L_{\mathrm{q}}(\varepsilon_{1,4,0})\cos^2(\theta/2) \approx \frac{8\Delta^2 g^2\Omega_p^2}{(\nu^3 - \nu\Omega_p^2)^2}, \\
L_{44,11} &= 2\sin^2(\theta/2) \approx \theta^2/2 \approx 2\Delta_1^2/\delta^2, \quad (33)
\end{aligned}$$

where the quantity L_{q} is given in Appendix A. Note that $L_{44,22} \gg L_{44,11}, L_{11,44}$. In this limit we find for the asymptotic density matrix elements

$$\begin{aligned}
\rho_{11}(\infty) &= \frac{L_{11,44}}{L_{11,44} + L_{44,11}}, \\
\rho_{22}(\infty) &= \rho_{33}(\infty) = 0, \\
\rho_{44}(\infty) &= 1 - \rho_{11}(\infty), \quad (34)
\end{aligned}$$

which gives the central result

$$\begin{aligned}
P_\infty &= \frac{\varepsilon_0}{\nu}\frac{L_{11,44} - L_{44,11}}{L_{11,44} + L_{44,11}} + O\left(V^2\right) \\
&\simeq \frac{\varepsilon_0}{\nu}\left(1 - \frac{2\Delta_1^2\nu^2(\nu^2 - \Omega_p^2)^2}{\Delta_1^2\nu^2(\nu^2 - \Omega_p^2)^2 + 4\Delta^2 g^2\Omega_p^2\delta^2}\right). \quad (35)
\end{aligned}$$

A comparison between the result of this formula and different numerical results, including those of an exact numerical ab-initio real-time QUAPI calculation [24–26], is shown in Figure 4. For the QUAPI-simulations, we have used the optimized parameters [26] $\Delta t = 0.23/\Delta$, $M = 12$ and $K = 1$. Moreover, we have applied an exponential cut-off for the Ohmic bath with a cut-off frequency $\omega_c = 10\Delta$ (since we are considering long-time stationary results, the explicit shape of the cut-off is irrelevant). Note that the picture of the TSS+HO being the central quantum system which is coupled to an Ohmic environment is particularly suited for QUAPI since the coherent dynamics of the central quantum system is treated exactly. A very good agreement, even near resonance, is found among all the used numerical schemes.

3.5 Results and discussion

To get a qualitative understanding of the results it is important to realize how the rates $L_{\alpha\beta,\alpha'\beta'}$ are formed. All Floquet states are superpositions of the four unperturbed states $|g,0\rangle$, $|g,1\rangle$, $|e,0\rangle$, $|e,1\rangle$. The rates $L_{\rm osc}$, $L_{\rm q}$, $L_{\rm q,osc}$ defined in equation (A.2) describe the time scales of the transitions between the different unperturbed states. In this discussion these will be called the basic transition rates. If we want to calculate the rates $L_{\alpha\alpha',\beta\beta'}$ which describe transitions between different Floquet states, we have to multiply the basic rates by the square of the amplitudes in the superpositions. For example the Floquet state $|\phi_1\rangle$ consists of an unperturbed state $|e,1\rangle$ with amplitude $\sin(\theta/2)$, and $|g,0\rangle$ with amplitude $\cos(\theta/2)$. The rate $L_{44,11}$ describing the dissipative transition from $|\phi_1\rangle$ to $|\phi_4\rangle$ has a term which is the basic transition rate from $|e,1\rangle$ to $|e,0\rangle$ ($L_{\rm osc}$) multiplied by $\sin^2(\theta/2)$, and a term which is the product of the basic transition rate from $|g,0\rangle$ to $|e,0\rangle$ ($L_{\rm q}$) and $\cos^2(\theta/2)$. In this qualitative explanation we can neglect the amplitudes of the other states in $|\phi_1\rangle$ and $|\phi_4\rangle$ which are $O(V^2)$.

Now we consider the rates at resonance. Here, the amplitudes $\sin(\theta/2)$ and $\cos(\theta/2)$ are equal and we only have to consider the largest basic rate which is $L_{\rm osc}$. The dominant transition from $|\phi_1\rangle$ to $|\phi_4\rangle$ is via the basic transition from $|e,1\rangle$ to $|e,0\rangle$ and it is fast (both amplitude in the superposition and rate $L_{\rm osc}$ are of order one). The same holds for the transitions between $|\phi_2\rangle$ to $|\phi_4\rangle$. There will also be a transition between $|\phi_3\rangle$ and $|\phi_1\rangle$, $|\phi_2\rangle$ via the basic transition between $|g,1\rangle$ and $|g,0\rangle$. Since only the decay of the oscillator plays a role, the stationary state is a thermally equilibrated mixture between $|e/g,1\rangle$ and $|e/g,0\rangle$ which is described by equation (32).

Away from resonance, the amplitude $\sin(\theta/2)$ becomes small ($\sim \Delta_1$) implying that other basic transitions start to play a role. The transition from $|\phi_2\rangle$ to $|\phi_4\rangle$ is still dominated by the basic transition from $|e,1\rangle$ to $|e,0\rangle$ with large amplitude $\cos(\theta/2)$. Within our assumption of low temperatures used to derive equation (35), the state $|\phi_2\rangle$ is weakly populated after long times. The same holds for $|\phi_3\rangle$. Between $|\phi_1\rangle$ and $|\phi_4\rangle$ two basic transitions are important. The first is a transition from $|e,1\rangle$ to $|e,0\rangle$ with large rate (i.e., fast) but low amplitude ($\sin(\theta/2)$) (i.e., rare). For low temperatures, this rate describes transitions from $|\phi_1\rangle$ to $|\phi_4\rangle$ and it dominates $L_{44,11}$ in equation (33). The other basic transition occurs via the unperturbed states $|e,0\rangle$ and $|g,0\rangle$. The basic rate $L_{\rm q}$ is small, but it has a large amplitude ($\cos(\theta/2)$). For low temperatures this mechanism causes transitions from $|\phi_4\rangle$ to $|\phi_1\rangle$ and it is the dominant part of $L_{11,44}$. The stationary state is described by the ratio of the rates as described by equation (35). Note that since both rates scale with g^2 the final result does not depend on g, for small g. For other resonances we find a different eigenvalue splitting and the peak shape will depend on g.

We will now try to give a more physical insight in the nature of this resonance. First consider the case when $T = 0$ and we are exactly on resonance. The driving induces transitions from $|g,0\rangle$ to $|e,1\rangle$ while the direct coupling of the HO to the environment will cause a fast decay of the population from $|e,1\rangle$ to $|e,0\rangle$. This transition from $|g,0\rangle$ to $|e,0\rangle$ via driving and decay has to compete with the decay from $|e,0\rangle$ to $|g,0\rangle$, but the last process is much slower because the TSS is not directly coupled to the environment. So all the population is in $|e,0\rangle$ and there is a complete inversion of population. For $T \neq 0$ there will be a thermal equilibrium between ground and excited state of the oscillator.

When the system is not exactly at resonance the driving induced transitions are much slower $\propto g^2$ and the decay of the oscillator is still fast. This means that the transition from $|g,0\rangle$ to $|e,0\rangle$ is slower than at resonance. The time associated with the decay from $|e,0\rangle$ to $|g,0\rangle$ is also $\propto g^2$ and the ratio of the time scales of the two processes gives the ratio of the populations of $|e,0\rangle$ and $|g,0\rangle$ (at $T = 0$, for higher T the states $|g/e,1\rangle$ are also populated). This ratio is independent of g and so is P_∞.

A similar analysis can be performed for the first red sideband at $\nu = \Omega + \Omega_p$. At resonance it yields $P_\infty = \frac{\varepsilon_0}{\nu}\tanh(\frac{\hbar\Omega_p}{2k_BT}) + O(V^2)$, which is very close to thermal equilibrium for low T.

For the resonance at $\nu = \Omega_p$, only the oscillator is excited. After having traced it out, we expect just thermal equilibrium given by $P_\infty = \frac{\varepsilon_0}{\nu}\tanh(\frac{\hbar\nu}{2k_BT})$.

4 Strong coupling: NIBA

In the complementary regime of large environmental coupling and/or high temperatures it is convenient to employ model (a), and it is appropriate to treat the system's dynamics within the noninteracting-blip approximation (NIBA) [8]. The NIBA is non-perturbative in the coupling α but perturbative in the tunneling splitting Δ. It is a good approximation for sufficiently high temperatures and/or dissipative strength, or for symmetric systems. Within the NIBA and in the limit of large driving frequencies $\Omega \gg \Delta$, one finds [9]

$$P_\infty = \frac{k_0^-(0)}{k_0^+(0)}. \tag{36}$$

Here,

$$k_0^-(0) = \Delta^2 \int_0^\infty dt h^-(t)\sin(\varepsilon_0 t) J_0\left(\frac{2s}{\Omega}\sin\frac{\Omega t}{2}\right),$$

$$k_0^+(0) = \Delta^2 \int_0^\infty dt h^+(t)\cos(\varepsilon_0 t) J_0\left(\frac{2s}{\Omega}\sin\frac{\Omega t}{2}\right), \tag{37}$$

with J_0 being the zeroth order Bessel function. Dissipative effects of the environment are captured by the terms

$$h^+(t) = e^{-Q'(t)}\cos[Q''(t)],$$
$$h^-(t) = e^{-Q'(t)}\sin[Q''(t)]. \tag{38}$$

Here, $Q'(t)$ and $Q''(t)$ are the real and imaginary parts of the bath correlation function

$$Q(t) = \int_0^\infty d\omega \frac{J(\omega)}{\omega^2}\,\frac{\cosh(\omega\beta/2) - \cosh[\omega(\beta/2 - it)]}{\sinh(\omega\beta/2)}.$$

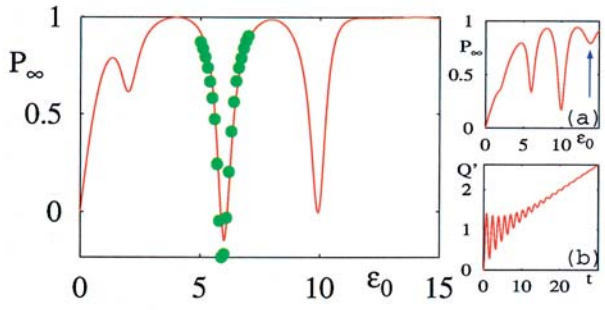

Fig. 5. P_∞ vs. ε_0 (in units of Δ). The solid line is the NIBA prediction, while the circles are from a QUAPI simulation with 6 HO levels ($g = 3\Delta$, $s = 4\Delta$, $\Omega = 10\Delta$, $\kappa = 0.014$, $k_BT = 0.5\hbar\Delta$, $\Omega_p = 4\Delta$). Inset (a): NIBA result for $k_BT = 2\hbar\Delta$. The arrows indicates the first red sideband at $\nu = \Omega + \Omega_p$. Inset (b): $Q'(t)$ vs. t shows damped oscillations.

For the peaked spectral density given in equation (4) one finds

$$Q'(t) = Q_1'(t) - e^{-\Gamma t}[Y_1\cos(\bar\Omega_p t) + Y_2\sin(\bar\Omega_p t)],$$
$$Q''(t) = A_1 - e^{-\Gamma t}[A_1\cos(\bar\Omega_p t) + A_2\sin(\bar\Omega_p t)]. \quad (39)$$

Here, $\beta = \hbar/k_BT, \Gamma = \pi\kappa\Omega_p$, $\bar\Omega_p^2 = \Omega_p^2 - \Gamma^2$ and

$$Q_1'(t) = Y_1 + \pi\alpha\Omega_p^2\left[\frac{\sinh(\beta\bar\Omega_p)t}{2C\bar\Omega_p} + \frac{\sin(\beta\Gamma)t}{2C\Gamma} - \frac{4\Omega_p^2}{\beta}\sum_{n=1}^{\infty}\frac{\frac{1}{\nu_n}[e^{-\nu_n t}-1]+t}{(\Omega_p^2+\nu_n^2)^2 - 4\Gamma^2\nu_n^2}\right], \quad (40)$$

where $\nu_n = 2\pi n/\beta$. Moreover, $C = \cosh(\beta\bar\Omega_p) - \cos(\beta\Gamma)$, $CY_{1/2} = \mp A_{2/1}\sinh(\beta\bar\Omega_p) - A_{1/2}\sin(\beta\Gamma)$, $A_2 = \alpha\pi(\Gamma^2 - \bar\Omega_p^2)/(2\Gamma\bar\Omega_p)$, $A_1 = \pi\alpha$. As follows from equation (39), Q' and Q'' display damped oscillations with frequency $\bar\Omega_p$ (cf. Fig. 5b) which are not present for a pure Ohmic spectrum. It is the interplay between these oscillations and the driving field which induces the extra resonances in P_∞.

To proceed, we rewrite the kernels $k_0^\pm(0)$ in a more convenient form. In the integrand of equation (37) the functions $\cos[Q''(t)]$, $\sin[Q''(t)]$ and $e^{-Q'(t)+Q_1'(t)}$ oscillate with frequency $\bar\Omega_p$ and we can expand them as

$$\cos[Q''(t)] = \sum_{m=-\infty}^{\infty}\left[D_m\cos(m\bar\Omega_p t) + E_m\sin(m\bar\Omega_p t)\right],$$
$$\sin[Q''(t)] = \sum_{m=-\infty}^{\infty}\left[F_m\cos(m\bar\Omega_p t) + G_m\sin(m\bar\Omega_p t)\right],$$
$$e^{-Q'(t)+Q_1'(t)} = \sum_{m=-\infty}^{\infty}\left[H_m\cos(m\bar\Omega_p t) + K_m\sin(m\bar\Omega_p t)\right]. \quad (41)$$

The coefficients D_m, E_m, F_m, G_m, H_m and K_m are time dependent and they are given in Appendix B. Inserting these expansions into equation (37), and also using the Fourier representation of $J_0\left(\frac{2s}{\Omega}\sin\frac{\Omega t}{2}\right)$, we find

$$k_0^\pm(0) = \sum_{m=-\infty}^{\infty}\sum_{n=-\infty}^{\infty}\Delta^2\int_0^\infty dt e^{-Q_1'(t)}f_{mn}^\pm(t). \quad (42)$$

Here, $\varepsilon_{mn} = \varepsilon_0 - m\bar\Omega_p - n\Omega$, and

$$f_{mn}^\pm(t) = \begin{matrix}\mathrm{Re}\\ \mathrm{Im}\end{matrix}\left[c_{mn}^\pm(t)\cos(\varepsilon_{mn}t) \pm c_{mn}^\mp(t)\sin(\varepsilon_{mn}t)\right],$$
$$c_{mn}^+ = J_n^2\left(\frac{s}{\Omega}\right)J_m(e^{-\Gamma t}\omega_1)\cos(m\phi)(-i)^m e^{-iA_1},$$
$$c_{mn}^- = J_n^2\left(\frac{s}{\Omega}\right)J_m(e^{-\Gamma t}\omega_1)\sin(m\phi)(-i)^m e^{-iA_1}, \quad (43)$$

with J_n being a Bessel function of order n, and

$$\omega_1 = \sqrt{(A_1 - iY_1)^2 + (A_2 - iY_2)^2},$$
$$\tan\phi = -\frac{A_2 - iY_2}{A_1 - iY_1}. \quad (44)$$

Thus, from equation (43), we expect resonances when $\varepsilon_{nm} = 0$.

In the limit $\Gamma/\Omega_p \ll 1$ and for not too large T (i.e., $\cos(\beta\Gamma) \ll \cosh(\beta\Omega_p)$), we find that

$$\tan(m\phi) \approx i\tanh\left(\frac{m\beta\Omega_p}{2}\right). \quad (45)$$

Inserting this into equation (43), we obtain

$$i\tanh\left(\frac{m\beta\Omega_p}{2}\right)c_{mn}^+ = c_{mn}^-. \quad (46)$$

If the environmental mode is enough localized (i.e., the integrand of Eq. (37) is only damped after several oscillations), we expect that the sum in equation (42) is dominated by the coefficient of $\cos\varepsilon_{nm}t$ if $\varepsilon_{mn} = 0$. This means that

$$f_{mn}^+(t) \approx \mathrm{Re}[c_{mn}^+(t)]$$
$$f_{mn}^-(t) \approx \tanh\left(\frac{m\beta\Omega_p}{2}\right)\mathrm{Re}[c_{mn}^+(t)], \quad (47)$$

which leads to

$$P_\infty = \tanh\left(\frac{m\beta\Omega_p}{2}\right). \quad (48)$$

Without driving we only have terms with $n = 0$ and $\varepsilon_{m0} = 0$ implies that $\varepsilon_0 = m\Omega_p$. In that case equation (48) gives the NIBA thermal equilibrium value. Hence, in order to find resonances we need to apply driving. For "conventional" resonances at $\varepsilon_0 = n\Omega$, we put m to zero and we find $P_\infty \approx 0$, as predicted for unstructured environments [17,27]. Finally, for $\varepsilon_0 = n\Omega \pm m\Omega_p$, we recover $P_\infty \approx \pm\tanh(m\beta\Omega_p/2)$, as was also found within the Floquet-Born-Markov approach, cf. (32). Results of a numerical evaluation of P_∞ are shown in Figure 5, using the NIBA result (43), as well as the exact ab-initio real-time QUAPI method [24–26]. Resonance dips are observed at $\varepsilon_0 = \Omega$, $\varepsilon_0 = \Omega - \Omega_p$ and $\varepsilon_0 = \Omega - 2\Omega_p$. For $k_BT \sim \hbar\Omega_p$, we also find the first red sideband at $\varepsilon_0 = \Omega + \Omega_p$, see inset (a).

$$P_\infty^{(n)}(\varepsilon_0) = \frac{\varepsilon_0\epsilon_n^2\Delta_0^2(\varepsilon_0^2+\Delta_0^2-\epsilon_n^2)\frac{J_{\rm Ohm}(\vartheta_0)}{\vartheta_0} + \varepsilon_0^2|\epsilon_n|\Delta_n^2(\epsilon_n^2+\Delta_n^2-\varepsilon_0^2)\frac{J_{\rm Ohm}(\vartheta_n)}{\vartheta_n}}{\Delta_0^2\epsilon_n^2(\varepsilon_0^2+\Delta_0^2-\epsilon_n^2)J_{\rm Ohm}(\vartheta_0)\coth\frac{\hbar\vartheta_0}{2k_BT} - \Delta_n^2\varepsilon_0^2(\epsilon_n^2+\Delta_n^2-\varepsilon_0^2)J_{\rm Ohm}(\vartheta_n)\coth\frac{\hbar\vartheta_n}{2k_BT}}. \quad (51)$$

5 Limit $\Omega_{\rm p} \gg \nu$

In the limit when the frequency Ω_p of the HO is much larger than the effective TSS level splitting ν, the peak in the spectral density at Ω_p acts as a high-frequency cut-off for an effective Ohmic bath, see equation (4). In other words, the oscillations in the correlation functions, see Section 4 which occur on a time-scale Ω_p^{-1} are very fast and can be averaged out when only the long-time dynamics is of interest and short-time effects are not considered. In this limit, the standard driven and Ohmically damped spin-boson model [8,9] is recovered. In the regime of weak damping $\alpha \ll 1$, the stationary population difference P_∞ has been determined within the assumption of large driving frequencies $\Omega \gg \Delta, ...$ upon using analytic real-time path integral methods in reference [27]. In this Section, we use this high-frequency approximation of reference [27] as a starting point, and derive a closed simple analytic expression for the peak shape of the "common" multi-photon resonance. Most importantly, we find the scaling of the width of the n-photon resonance as the nth Bessel function $J_n(s/\Omega)$. This scaling behavior has been observed experimentally in superconducting flux qubit devices [16].

The central issue in finding a closed analytic expression for P_∞ is to find the roots ϑ_n of the pole equation [27]

$$\prod_{n=-\infty}^{+\infty}\left(\epsilon_n^2-\vartheta^2\right)+\sum_{n=0}^{+\infty}\Delta_n^2\prod_{m=-\infty,m\neq n}^{+\infty}\left(\epsilon_m^2-\vartheta^2\right)=0. \quad (49)$$

Here, $\epsilon_n = \varepsilon_0 - n\Omega$ is the photon-induced bias and $\Delta_n = |J_n(s/\Omega)|\Delta$ is the field-dressed tunneling splitting of the TSS, where $J_n(x)$ is the nth ordinary Bessel function. Considering the n-photon resonance, we numerically find that, up to extremely high numerical precision, the roots of equation (49) are given by

$$\begin{aligned}\vartheta_0 &= \sqrt{\varepsilon_0^2+\Delta_0^2},\\ \vartheta_{n\neq 0} &= \sqrt{\epsilon_n^2+\Delta_n^2},\\ \vartheta_{k\neq n,0} &= \epsilon_k. \end{aligned} \quad (50)$$

Plugging equations (50) in the expressions for P_∞ given in reference [27], see equations (6) and (7) therein, we find a closed expression for the lineshape of the n-photon resonance to be

See equation (51) above.

This result can be simplified upon observing that the second term in the numerator is small if the driving is not too large, since then $\Delta_n^2 \ll \Delta_0^2$. Moreover, we are interested in the regime $\epsilon_0 \gg \Delta$ which is the saturation regime implying that $\nu \approx \varepsilon_0$ and at low temperatures. Then, away from the resonance point at $n\Omega \approx \varepsilon_0$, the second term in the denominator in equation (51) can be neglected and one recovers the standard result, if one uses that $\Delta_0 \approx \Delta$ which is fulfilled for weak driving. It reads

$$P_\infty^{(n)}(\varepsilon_0) = \frac{\varepsilon_0}{\sqrt{\varepsilon_0^2+\Delta^2}}\tanh\frac{\sqrt{\varepsilon_0^2+\Delta^2}}{2k_BT}, \quad (52)$$

which gives the correct result away from any n-photon resonance. For the case at the n-photon resonance at $n\Omega \approx \varepsilon_0$, one finds a Lorentzian line shape, i.e.,

$$P_\infty^{(n)}(\varepsilon_0) = \frac{\Delta_0^2(\varepsilon_0-n\Omega)^2}{\Delta_0^2(\varepsilon_0-n\Omega)^2+2\varepsilon_0^2\Delta_n^2k_BT/\hbar}, \quad (53)$$

where we have expanded the second coth term in the denominator (see Eq. (51)) up to lowest order in the argument, which is appropriate since ϑ_n is small at resonance (and at low temperature). The linewidth of the Lorentzian peak can be calculated as the full width at half maximum (FWHM)

$$\Delta\varepsilon^{(n)} = 2\sqrt{2n\Omega\left(\frac{\Delta_n}{\Delta_0}\right)^2\frac{k_BT}{\hbar}+\left(\frac{\Delta_n}{\Delta_0}\right)^4\left(\frac{k_BT}{\hbar}\right)^2}. \quad (54)$$

Note that this result obtained from the high-frequency approximation is independent of the damping constant. Moreover, the leading term is the first term under the square root in equation (54). Note furthermore that for the case of infinitesimal driving, the FWHM is not correctly reproduced by equation (54) since it would approach zero. However, as it is known from NMR within a treatment in terms of the Bloch equation, in this case, the FWHM is dominated by the dephasing [17], i.e.,

$$\Delta\varepsilon_{\rm Bloch}^{(1)} = 2\sqrt{\Gamma_\phi^2+\Omega_R^2\Gamma_\phi/\Gamma_R}, \quad (55)$$

where $\Gamma_R = \pi\alpha\coth(\hbar\nu/2k_BT)\Delta^2/\nu$ is the relaxation rate and $\Gamma_\phi = \Gamma_R/2 + 2\pi\alpha(\varepsilon_0^2/\nu^2)k_BT/\hbar$ [8]. Both rates are of first order in the damping strength α. Moreover, Ω_R is the (single-photon) Rabi frequency. Hence, we have to include the dephasing rate Γ_ϕ^2 in equation (53), since it cannot be reproduced by our weak-coupling approach which is only of first order in α. This finally yields in leading order in the driving strength

$$\Delta\varepsilon^{(n)} = 2\sqrt{\Gamma_\phi^2+\left(\frac{\Delta_n}{\Delta_0}\right)^2 2n\Omega\frac{k_BT}{\hbar}}. \quad (56)$$

As follows from equation (56), the FWHM of the n-photon resonance scales with the nth ordinary Bessel function, i.e., $\Delta\varepsilon^{(n)} \sim J_n(s/\Omega)$ as also confirmed by experimental measurements [16].

$$
\begin{aligned}
&L_{11,22} = L_{22,11} = L_{33,44} = L_{44,33} = 0, \quad L_{11,11} = -(L_{33,11} + L_{44,11}),\\
&L_{22,22} = -(L_{33,22} + L_{44,22}), \quad L_{33,33} = -(L_{11,33} + L_{44,33}),\\
&L_{44,44} = -(L_{11,44} + L_{22,44}), \quad L_{12,12} = (L_{22,22} + L_{11,11})/2, \quad L_{11,33} = L_{44,22},\\
&L_{22,33} = L_{44,11}, \quad L_{33,22} = L_{11,44}, \quad L_{33,11} = L_{22,44}, \quad L_{22,21} = L_{21,11},\\
&L_{11,21} = L_{21,22}, \quad L_{44,21} = -L_{21,33}, \quad L_{33,21} = -L_{21,44}, \quad L_{22,12} = L_{22,21},\\
&L_{11,12} = L_{11,21}, \quad L_{44,12} = L_{44,21}, \quad L_{33,21} = L_{33,12}, \quad L_{12,21} = 0.
\end{aligned} \tag{A.1}
$$

$$
\begin{aligned}
L_{44,22} &= 2L_{\rm osc}(\varepsilon_{4,2,-1})\cos^2\left(\frac{\theta}{2}\right) + 2L_{\rm q}(\varepsilon_{4,2,0})\sin^2\left(\frac{\theta}{2}\right) - L_{\rm q,osc}(\varepsilon_{4,2,-1})\sin\theta,\\
L_{22,44} &= 2L_{\rm osc}(\varepsilon_{2,4,1})\cos^2\left(\frac{\theta}{2}\right) + 2L_{\rm q}(\varepsilon_{2,4,0})\sin^2\left(\frac{\theta}{2}\right) - L_{\rm q,osc}(\varepsilon_{2,4,1})\sin\theta,\\
L_{44,11} &= 2L_{\rm osc}(\varepsilon_{4,1,-1})\sin^2\left(\frac{\theta}{2}\right) + 2L_{\rm q}(\varepsilon_{4,1,0})\cos^2\left(\frac{\theta}{2}\right) + L_{\rm q,osc}(\varepsilon_{4,1,-1})\sin\theta,\\
L_{11,44} &= 2L_{\rm osc}(\varepsilon_{1,4,1})\sin^2\left(\frac{\theta}{2}\right) + 2L_{\rm q}(\varepsilon_{1,4,0})\cos^2\left(\frac{\theta}{2}\right) + L_{\rm q,osc}(\varepsilon_{1,4,1})\sin\theta,\\
L_{21,22} &= \frac{1}{2}\left(L_{\rm osc}(\varepsilon_{3,2,0}) - L_{\rm q}(\varepsilon_{3,2,-1}) - L_{\rm osc}(\varepsilon_{4,2,-1}) + L_{\rm q}(\varepsilon_{4,2,0})\right)\sin\theta + \frac{1}{2}(L_{\rm q,osc}(\varepsilon_{3,2,0}) - L_{\rm q,osc}(\varepsilon_{4,2,-1}))\cos\theta,\\
L_{21,11} &= \frac{1}{2}\left(L_{\rm osc}(\varepsilon_{3,1,0}) - L_{\rm q}(\varepsilon_{3,1,-1}) - L_{\rm osc}(\varepsilon_{4,1,-1}) + L_{\rm q}(\varepsilon_{4,1,0})\right)\sin\theta + \frac{1}{2}(L_{\rm q,osc}(\varepsilon_{3,1,0}) - L_{\rm q,osc}(\varepsilon_{4,1,-1}))\cos\theta,\\
L_{21,44} &= \frac{1}{2}\left(L_{\rm osc}(\varepsilon_{1,4,1}) + L_{\rm osc}(\varepsilon_{2,4,1}) - L_{\rm q}(\varepsilon_{1,4,0}) - L_{\rm q}(\varepsilon_{2,4,0})\right)\sin\theta + \frac{1}{2}(L_{\rm q,osc}(\varepsilon_{1,4,1}) + L_{\rm q,osc}(\varepsilon_{2,4,1}))\cos\theta,\\
L_{21,33} &= \frac{1}{2}\left(L_{\rm q}(\varepsilon_{1,3,1}) + L_{\rm q}(\varepsilon_{2,3,1}) - L_{\rm osc}(\varepsilon_{1,3,0}) - L_{\rm osc}(\varepsilon_{2,3,0})\right)\sin\theta - \frac{1}{2}(L_{\rm q,osc}(\varepsilon_{1,3,0}) + L_{\rm q,osc}(\varepsilon_{2,3,0}))\cos\theta,
\end{aligned}
$$

6 Conclusions

In conclusion we have investigated the problem of a quantum mechanical driven two-state system being coupled to a structured environment which has a localized mode at a frequency Ω_p but behaves Ohmically at low frequencies. We have studied two complementary parameter regimes of weak and strong coupling to the environment. The interplay of the driving and the localized mode gives additional features like resonant peaks/dips in the asymptotic averaged population difference P_∞. We have calculated analytically the lineshape of the resonances in various parameter regimes and have obtained simple closed expressions for the particular example of the first blue sideband. We also include the discussion of how the results are generalized for any sideband. Moreover, we have elaborated the limit when the localized mode acts as a high-frequency cut-off. Then, the full width at half maximum of the n-photon resonance has been shown to scale with the nth ordinary Bessel function.

Our model finds as well applications in the field of cavity quantum electrodynamics (CQED) with solid state structures [28]. Most interestingly, the strong coupling limit of CQED could be reached in superconducting electrical circuits, with perspective applications ahead.

Finally, we note that a related experiment has been reported recently by Wallraff et al. [29]. There, a qubit was realized in the form of a Cooper pair box which couples to a single mode of a cavity which is damped. The properties of the TSS-HO were probed spectroscopically by measuring the transmission of the resonator. In other words, a *driven* HO was considered while the TSS was kept static. In contrast to that system, here, the TSS was time-dependent while the HO is treated as static.

We thank P. Bertet, I. Chiorescu and H. Mooij for discussions. This work has been supported by the Universitätsstiftung Hans Vielberth and the Dutch NWO/FOM.

Appendix A: Symmetry properties for the dissipative rates for the first blue sideband

In order to evaluate the stationary averaged population difference P_∞, the rate coefficients $L_{\alpha\beta,\alpha'\beta'}$ have to be determined explicitly. For the example of the resonance at $\nu \approx \Omega - \Omega_p$ (first blue sideband) considered in this work, we find that the rate coefficients fulfill the symmetry relations

See equation (A.1) above.

As a consequence, there are eight independent rates given by

See equation above,

with

$$
\begin{aligned}
L_{\rm q}(\varepsilon_{klm}) &= \langle e,1,0|e^{iS}Xe^{-iS}|g,1,0\rangle^2 N(\varepsilon_{klm}) \\
&= \langle e,0,0|e^{iS}Xe^{-iS}|g,0,0\rangle^2 N(\varepsilon_{klm}) \\
&= \frac{4g^2\Delta^2\Omega_p^2 N(\varepsilon_{klm})}{\nu^2(\nu^2-\Omega_p^2)^2}, \\
L_{\rm osc}(\varepsilon_{klm}) &= \langle g,1,0|e^{iS}Xe^{-iS}|g,0,0\rangle^2 N(\varepsilon_{klm}) \\
&= \langle e,1,0|e^{iS}Xe^{-iS}|e,0,0\rangle^2 N(\varepsilon_{klm}) \\
&= \left(\frac{4g^2(\Delta^2(\nu^2-2\Omega_p^2)-(\nu^2-\Omega_p^2)^2)}{\Omega_p^2(\nu^2-\Omega_p^2)^2}+1\right) \\
&\quad \times N(\varepsilon_{klm}), \\
L_{\rm q,osc}(\varepsilon_{klm}) &= -2\langle e,1,-1|e^{iS}Xe^{-iS}|g,1,0\rangle \\
&\quad \times \langle g,1,0|e^{iS}Xe^{-iS}|g,0,0\rangle N(\varepsilon_{klm}) \\
&= 2\langle g,0,1|e^{iS}Xe^{-iS}|e,0,0\rangle \\
&\quad \times \langle e,0,0|e^{iS}Xe^{-iS}|e,1,0\rangle N(\varepsilon_{klm}) \\
&= \frac{\Delta\varepsilon_0 gs((\Omega+\Omega_p)^2+2\Omega_p^2+\nu(-\Omega+\Omega_p))N(\varepsilon_{klm})}{2\nu(\nu-\Omega)\Omega(\nu-\Omega-\Omega_p)\Omega_p(\nu+\Omega_p)}, \\
N(\varepsilon_{klm}) &= N(\varepsilon_k-\varepsilon_l+m\Omega). \qquad \text{(A.2)}
\end{aligned}
$$

Note that $L_{\rm osc}$ is the rate containing the zeroth order term in g and s. It is related to the transition between two states differing by one oscillator quantum. This decay is of zeroth order (hence fast) because the oscillator is coupled directly to the environment. Moreover, $L_{\rm q}$ gives the rate for transitions between the excited and ground state of the TSS with the HO remaining in the same state, and $L_{\rm q,osc}$ is related to the transition where both the qubit and the oscillator exchange energy with the environment. Note that this transition is induced by the driving and involves one photon.

Appendix B: Coefficients for the kernels $\mathbf{k_0^{\pm}(0)}$

In Section 4, we have introduced an expansion of the oscillating functions given in equation (41). In this appendix we summarize the corresponding coefficients for completeness.

For the expansion of $\cos[Q''(t)]$, we find

$$
\begin{aligned}
D_{2m+1} &= (-1)^m \sin(A_1) J_{2m+1}(A) \cos[(2m+1)X], \\
D_{2m} &= (-1)^m \cos(A_1) J_{2m}(A) \cos(2mX), \\
E_{2m+1} &= (-1)^m \sin(A_1) J_{2m+1}(A) \sin[(2m+1)X], \\
E_{2m} &= (-1)^m \cos(A_1) J_{2m}(A) \sin(2mX), \qquad \text{(B.1)}
\end{aligned}
$$

where we have introduced

$$
\begin{aligned}
A &= e^{-\Gamma t}\sqrt{A_1^2+A_2^2}, \\
\sin X &= A_2/\sqrt{A_1^2+A_2^2}. \qquad \text{(B.2)}
\end{aligned}
$$

In the same way, the expansion of $\sin[Q''(t)]$ gives

$$
\begin{aligned}
F_{2m+1} &= (-1)^{m+1} \cos(A_1) J_{2m+1}(A) \cos[(2m+1)X], \\
F_{2m} &= (-1)^m \sin(A_1) J_{2m}(A) \cos[2mX], \\
G_{2m+1} &= (-1)^{m+1} \cos(A_1) J_{2m+1}(A) \sin([2m+1)X], \\
G_{2m} &= (-1)^m \sin(A_1) J_{2m}(A) \sin[2mX]. \qquad \text{(B.3)}
\end{aligned}
$$

Finally, we find for the coefficients of $\exp[Q(t)-Q_1(t)]$

$$
\begin{aligned}
H_m &= I_m(Y)\cos(mV), \\
K_m &= I_m(Y)\sin(mV), \qquad \text{(B.4)}
\end{aligned}
$$

where we have introduced

$$
\begin{aligned}
Y &= e^{-\Gamma t}\sqrt{Y_1^2+Y_2^2}, \\
\tan V &= \frac{Y_2}{Y_1}. \qquad \text{(B.5)}
\end{aligned}
$$

Here, I_m is the modified Bessel function of the first kind of order m.

References

1. Y. Nakamura, Yu.A. Pashkin, J.S. Tsai, Nature **398**, 786 (1999)
2. J.M. Martinis, S. Nam, J. Aumentado, C. Urbina, Phys. Rev. Lett. **89**, 117901 (2002)
3. Yu.A. Pashkin, T. Yamamoto, O. Astafiev, Y. Nakamura, D.V. Averin, J.S. Tsai, Nature **421**, 823 (2003)
4. D. Vion, A. Aassime, A. Cottet, P. Joyez, H. Pothier, C. Urbina, D. Esteve, M.H. Devoret, Science **296**, 886 (2002)
5. I. Chiorescu, Y. Nakamura, C.J.P.M. Harmans, J.E. Mooij, Science **299**, 1869 (2003)
6. I. Chiorescu, P. Bertet, K. Semba, Y. Nakamura, C.J.P.M. Harmans, J.E. Mooij, Nature **431**, 159 (2004)
7. C. Cohen-Tannoudji, J. Dupont-Roc, G. Grynberg, *Atom-Photon Interactions* (Wiley, New York, 1992)
8. U. Weiss, *Quantum Dissipative Systems* (World Scientific, Singapore, 1999)
9. M. Grifoni, P. Hänggi, Phys. Rep. **304**, 229 (1998)
10. L. Tian, S. Lloyd, T.P. Orlando, Phys. Rev. B **65**, 144516 (2002)
11. M. Thorwart, L. Hartmann, I. Goychuk, P. Hänggi, J. Mod. Opt. **47**, 2905 (2000)
12. A.Yu. Smirnov, Phys. Rev. B **67**, 155104 (2003)
13. M. Thorwart, E. Paladino, M. Grifoni, Chem. Phys. **296**, 333 (2004)
14. F.K. Wilhelm, S. Kleff, J. von Delft, Chem. Phys. **296**, 345 (2004)
15. S. Kleff, S. Kehrein, J. von Delft, Phys. Rev. B **70**, 014516 (2004)
16. S. Saito, M. Thorwart, H. Tanaka, M. Ueda, H. Nakano, K. Semba, H. Takayanagi, Phys. Rev. Lett. **93**, 037001 (2004)

17. M.C. Goorden, F.K. Wilhelm, Phys. Rev. B **68**, 012508 (2003)
18. M.C. Goorden, M. Thorwart, M. Grifoni, Phys. Rev. Lett. **93**, 267005 (2004)
19. A. Garg, J.N. Onuchic, V. Ambegaokar, J. Chem. Phys. **83**, 4491 (1985)
20. R. Blümel, R. Graham, L. Sirko, U. Smilansky, H. Walther, K. Yamada, Phys. Rev. Lett. **62**, 341 (1989)
21. S. Kohler, T. Dittrich, P. Hänggi, Phys. Rev. E **55**, 300 (1997)
22. J.H. Shirley, Phys. Rev. **138**, B979 (1965)
23. I. Shavit, L.T. Redmon, J. Chem. Phys. **73**, 5711 (1980)
24. N. Makri, D.E. Makarov, J. Chem. Phys. **102**, 4600 (1995)
25. M. Thorwart, P. Reimann, P. Jung, R.F. Fox, Chem. Phys. **235**, 61 (1998)
26. M. Thorwart, P. Reimann, P. Hänggi, Phys. Rev. E **62**, 5808 (2000)
27. L. Hartmann, I. Goychuk, M. Grifoni, P. Hänggi, Phys. Rev. E **61**, R4687 (2000)
28. S.M. Girvin, R.-S. Huang, A. Blais, A. Wallraff, R.J. Schoelkopf, in *Proceedings of Les Houches Summer School*, Session LXXIX, Quantum Entanglement and Information Processing (2003); see also `cond-mat/0310670`
29. A. Wallraff, D.I. Schuster, A. Blais, L. Frunzio, R.-S. Huang, J. Majer, S. Kumar, S.M. Girvin, R.J. Schoelkopf, Nature **431**, 162 (2004)